Journal of Climate Change
ISSN 2395-7611 Volume 12 (2026) No. 1. pp. 46-59

https://doi.org/10.70917/jcc-2026-003

Article

Local Hydroclimatic Variability and Teleconnectivity Related to Warm and Cold Phases of Atmosphere-Ocean Coupled Circulation

Jai Hong Lee [1,*], Woochul Kang [2], Yoohyun Beck [3] and Gwangjin Jang [4]

[1] Department of Engineering, South Carolina State University, Orangeburg, SC, USA
[2] Department of Smart Infrastructure Engineering, Cheonan College of Engineering, Kongju National University, Cheonan, 31080, Republic of Korea
[3] Department of Civil and Architectural Engineering, Seokyeong University, Seoul, 02713, Republic of Korea
[4] Disaster Prevention Research Lab, National Disaster Management Research Institute, Ulsan, 44538, Republic of Korea
* Corresponding author: civilcolostate.edu@gmail.com; +1-803-536-8858

Abstract: Deciphering the El Niño/Southern Oscillation (ENSO) influences on hydroclimatic factors in both tropical and extratropical regions is crucial. This study employed empirical methods to identify areas with consistent hydroclimatic signals in relation to extreme ENSO phases. We examined the climatic linkages between ENSO's warm and cold phases and local temperature patterns across Southeastern US. Spatial coherence values were calculated using monthly temperature composites over a 2-year ENSO cycle, and candidate regions were identified using the first harmonic fit. Temporal consistency rates were determined through aggregate composites and index time series (ITS) to pinpoint core regions. This study identified two core regions: Western Inland Region (WIR) and Easter Coastal Region (ECR), with the WIR showing the more significant response to both warm and cold ENSO forcings. During ENSO warm (cold) years, temperature composites showed below (above) normal levels in these regions from winter to spring. Spatial coherence rates for El Niño (La Niña) in WIR and ECR were 0.97 to 0.98 (0.97 to 0.99), and temporal consistency rates ranged from 0.72 to 0.76 (0.82 to 0.86). Composite-harmonic analysis revealed that temperature anomalies tend to reverse signs between opposite ENSO phases, with positive anomalies in warm years showing more coherence and stronger responses compared to negative anomalies in cold years. The findings indicate that Southeastern US temperature patterns are significantly influenced by ENSO, highlighting a climatic teleconnection between El Niño and La Niña events and local middle latitude temperature.

Keywords: El Niño/Southern Oscillation; temperature; teleconnection

1. Introduction

The El Niño Southern Oscillation (ENSO) is a recurring climate pattern linked to temperature changes in the Equatorial Pacific, affecting central and eastern tropical Pacific Ocean regions. The ENSO cycle, lasting from 1 to 7 years, involves temperature variations of 1 to 3 degrees, with El Niño and La Niña representing its extreme phases (WMO, 2014). El Niño, which means “Little Boy” in Spanish, occurs due to weakened trade winds leading to the warming of ocean temperatures in the Equatorial Pacific, including central and eastern tropical regions. This warming causes warm water to reach the western coast of the Americas, shifting the Pacific jet stream southward and resulting in increased flooding and rainfall in the Southeast United States, along with drier conditions in the northern U.S. Conversely, La Niña, meaning “Little Girl” in Spanish, involves the cooling of ocean temperatures in the central and eastern tropical Pacific as strong trade winds push warm water westward toward Asia. This cooling often leads to upwelling along the western coast of the Americas, causing rain and flooding in the northern U.S. and droughts in the southern U.S. The Southern Oscillation refers to the sea level pressure

difference between Tahiti and Darwin, driving large-scale air pressure changes.

Many studies have examined these phenomena on global and regional scales, exploring naturally occurring events. Consequently, these investigations have amassed extensive information on ENSO's effects, including major climatic extremes like heat/cold waves, heavy precipitation, tropical cyclones, and droughts worldwide. This data has facilitated the development of various scientific methods to predict and prepare for hazardous events. The Southern Oscillation's impact on Indian hydroclimatic variability first studied by (Walker et al., 1923; Walker et al., 1932). Since then, many global studies have explored ENSO's extreme phases, identifying significant links between these phases and global temperature patterns. Berlage (1966) found a strong correlation between ENSO extreme events and global temperature anomaly, while Rasmusson and Carpenter (1983) linked Southern Oscillation phases to temperature patterns. Bradley et al. (1987) identified notable ENSO-related temperature signals using a set of high-quality temperature time series. Halpert and Ropelewski (1992) examined spatiotemporal ranges, finding consistent global temperature responses to both ENSO extreme phases. Kiladis and Diaz (1989) confirmed these strong correlations between ENSO phases and temperature anomalies. More recently, Davey (2014) plotted global spatial maps to categorize the temporal and spatial patterns of typical land temperature responses to the warm phase of ENSO events using the rate of occurrence analysis results. Regional studies have demonstrated ENSO's impact on low and middle latitude climatic variability, including those by Van Loon et al. (1981), Ropelewski et al. (1986), Redmond et al. (1988), and Kiladis et al. (1989). Several studies have shown a correlation between ENSO phases and temperature on a midlatitude regional scale. In the United States, Van Loon et al. (1981) found that significant stability of correlation between sea level pressure and the Southern Oscillation and surface air temperature in the northern winter. Ropelewski et al. (1986) explored the climatic linkages between North American temperature patterns and extreme southern oscillation, revealing ENSO-related patterns, a finding supported by Kiladis et al. (1989). They examined the impacts of extreme phases of Southern Oscillation (SO) on Indian temperature patterns on a monthly basis. Lee et al. (2018) identified areas in the Korean Peninsula where temperature anomalies statistically correlated with both ENSO phases. Viet (2021) analyzed the relationship between ENSO effects and temperature over the southern Vietnam region and developed a new ENSO index for the proposed area, namely, southern Vietnam ENSO Index (VEI). Tamaddun et al. (2019) studied the northern India focusing on the relationship between regional surface temperature and ENSO episodes during monsoon season and documented that the warm event years played a greater role in causing temperature changes than the cold or neutral phases. Kemarau and Eboy (2022) used Oceanic Niño Index (ONI) values to investigate ENSO's impact on temperature patterns over Kuching region in Malaysia. They employed linear regression for predicting ENSO-related temperature signals and revealed some notable findings for understanding the ENSO-temperature relationship in urban areas.

As demonstrated, numerous studies have investigated ENSO on global and regional scales. Despite extensive research into ENSO-related climate teleconnections, there is limited knowledge about ENSO events on localized temperature variation. Recently, temperature has become more intensified and localized, leading to devastating effects, including heat waves and hydrologic extremes that impact both the natural environment and human life and property. Analyzing how extreme phases of climatic variation influence local temperature patterns is essential for predicting and preparing for natural hazards. Therefore, it is crucial to systematically study how the extreme phases of ENSO events (El Niño and La Niña) affect local temperature patterns in Southeastern US. The study on ENSO-related temperature variability in the Southeastern US offers valuable insights for climate adaptation across various sectors. By understanding how temperature patterns shift with ENSO phases, targeted adaptation strategies can be developed in terms of agriculture, energy, public health, water management, and urban planning. For example, Farmers can align planting seasons and crop choices with cooler El Niño and warmer La Niña years, optimizing yields and minimizing risks. Utility can anticipate and manage seasonal demand for heating and cooling based on ENSO forecasts, aiding grid resilience. Local governments can prepare heat and cold exposure strategies for vulnerable populations according to ENSO-driven temperature changes. Also, warmer temperatures during La Niña years may stress water resources, making early conservation planning essential. From the perspective of urban Planning, ENSO patterns can guide infrastructure investments in heat resilience and cooling amenities in cities. Overall, integrating ENSO-based temperature insights into policy can strengthen regional climate resilience by enabling proactive responses to expected temperature variability. The present study aims at providing updated hydroclimatic data on spatiotemporal extent and intensity of ENSO-related temperature signals at various locations across the state. The primary goal of the present study is to examine the variability of temperature in Southeastern US in relation to the extreme phases of ENSO forcing through composite and harmonic analysis. This research explores the intensity, timing, and spatial boundaries of the ENSO-temperature correlation by examining temporal cycles and spatial patterns. Additionally, the present

study demonstrates comparative interpretation for two types of teleconnections triggered by the warm and cold phases of ENSO events (El Niño and La Niña), focusing on the magnitude and temporal phases of the climatic signals using cross-correlation analysis and annual cycle analysis.

2. Data and Analysis

2.1. Data and Study Area

The study utilizes monthly temperature data from 146 climate divisions across Southeastern US, sourced from the National Center for Environmental Information (NCEI), a division of NOAA responsible for U.S. meteorological monitoring (Figure 1). Spanning from 1895 to 2020, the dataset includes periods of 29 El Niño and 22 La Niña events, capturing extreme phases of historical ENSO episodes. To assess ENSO's consistent impact on temperature anomalies across the study area, two sets (El Niño and La Niña) of extreme ENSO phases were chosen based on criteria outlined by Ropelewski et al. (1987, 1989), Rasmusson et al. (1983), and Kiladis et al. (1989). These episodes are detailed in Table 1. The Southern Oscillation Index (SOI), derived from NOAA's Climate Prediction Center, is employed to gauge large-scale climate variations in the central and eastern areas of Pacific Ocean. SOI calculations are based on standardized differences in sea level pressure anomalies between Darwin and Tahiti. Focusing on the proposed midlatitude area in the Southeastern US allows for a more detailed understanding of the local impact of large-scale climate circulations like ENSO. This proposed area represents distinct geographical and climatic zones within the Southeast, providing a clearer view of how ENSO's temperature effects vary locally. By narrowing the scope, the study avoids diluting specific regional patterns that could be masked by broader, more heterogeneous areas. This localized focus enables more precise insights into temperature variability and its implications for regional climate adaptation strategies.

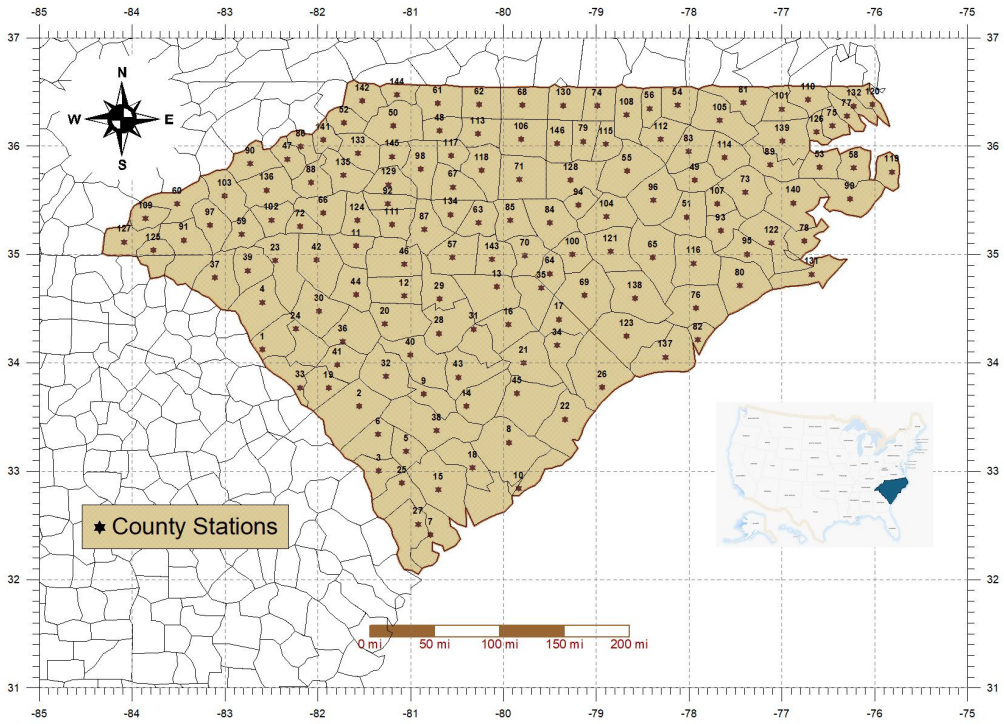

Figure 1. Climate divisions for temperature data.

Table 1. List of the ENSO episode years.

El Niño years	La Niña years
1905, 1911, 1914, 1918, 1923, 1925, 1930, 1932, 1939, 1941, 1951, 1953, 1957, 1963, 1965, 1969, 1972, 1976, 1982, 1986, 1991, 1994, 1997, 2002, 2004, 2006, 2009, 2015, 2018.	1910, 1915, 1917, 1924, 1928, 1938, 1950, 1955, 1964, 1971, 1973, 1975, 1985, 1988, 1995, 1998, 2000, 2005, 2007, 2010, 2011, 2017

2.2. Analysis

To explore how the extreme ENSO forcing influence temperature patterns across the study area, this study applies empirical methods employed by Ropelewski and Halpert (1986), cross-correlation analysis, and annual cycle analysis with modifications and enhancements. Figure 2 outlines the analysis process in three stages: initial data processing to convert raw data into appropriate formats like ranked percentiles, modular coefficients, and categorized SOIs; followed by core region identification through composite and harmonic analyses; and concluding with comparisons of the ENSO-related temperature signals using annual cycle analysis and lead-lag correlation analysis. Monthly temperature data undergo transformation into modular coefficients for annual cycle analysis, standardizing values by eliminating variance and mean effects. Temperature values are expressed as percentages relative to annual averages, ensuring all divisions maintain consistent cyclic representation. In this analysis, lead-lag correlation coefficients are calculated seasonally for temperature percentile and categorized STIs. Four seasonal datasets, i.e., Dec-Feb, Mar-May, Jun-Aug, and Sep-Nov, are generated by averaging three-month values. SOI values are divided into five categories based on their magnitudes, namely, strong cold, weak cold, normal phase, weak warm, and strong warm. Seasonal temperature time series are then transformed into percentile ranked probability data based on the Weibull plotting position technique, removing periodic trends and addressing disparities among climate divisions. Monthly temperature data are ranked in ascending order and normalized by (n+1), where (n) denotes the dataset size.

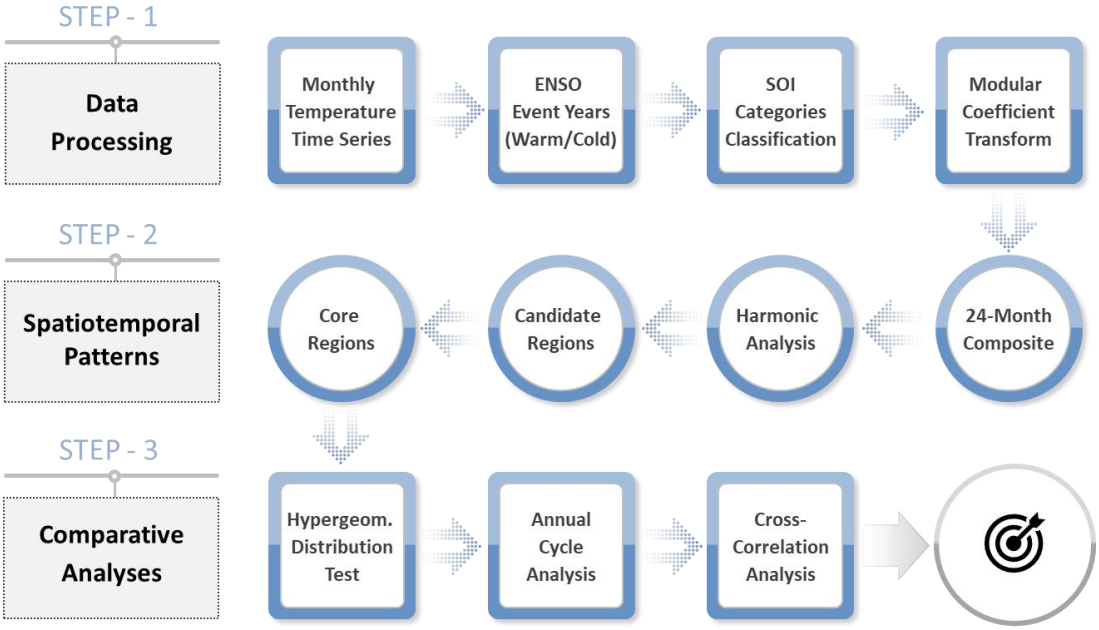

Figure 2. Methodological Approach.

2.3. Composite and Harmonic Analysis

For each climatic zone, monthly temperature percentile composites are calculated over a 24-month period, starting from July before the event year to June after, for both positive and negative phases of the Southern Oscillation (SO). July before the event is labeled as Jul (−), and June following the event year as Jun (+). Separate composites are computed for each SO phase, fitting them with the first harmonic of a theoretical 2-year SO period (either high or low phases). This approach follows the assumption; one temperature peak/trough during an SO event and that the SO aligns with the annual cycle (Figure 3). A 2-year cycle was employed as it encompasses a full cycle of an SO phase (Rasmusson and Carpenter, 1983). In the first harmonic cycle, the amplitude indicates the strength of temperature signals linked to ENSO, and the peak timing from the mean value is represented by the angular phase as shown in Figure 4. The theoretical background of the harmonic fits are based on Fourier Transform as follows (Wilks, 1995).

$$P_t = \overline{P} + \sum_{i=1}^{n/2}\left\{C_i \cos\left[\frac{2\pi it}{N} - \beta_i\right]\right\} = \overline{P} + \sum_{i=1}^{n/2}\left\{A_i \cos\left[\frac{2\pi it}{n}\right] + B_i \sin\left[\frac{2\pi it}{n}\right]\right\} \quad (1)$$

$$A_i = \frac{2}{n}\sum_{t=1}^{n} y_t \cos\left(\frac{2\pi i t}{n}\right), \quad B_i = \frac{2}{n}\sum_{t=1}^{n} y_t \sin\left(\frac{2\pi i t}{n}\right), \quad C_i = \left(A_i^{\,2} + B_i^{\,2}\right)^{0.5} \tag{2}$$

$$\beta_i = \tan^{-1}\frac{B_i}{A_i}\ (A_i > 0), \quad \frac{\pi}{2}\ (A_i = 0), \quad \tan^{-1}\frac{B_i}{A_i} \pm \pi\ (A_i < 0) \tag{3}$$

where P_t and $\overline{P}$ are the monthly and mean temperature, C_i is magnitude of harmonic curve, β_i is peak time of harmonic curve, and A_i and B_i are Fourier coefficients. The temporal phase and amplitude of the harmonic curve are depicted as vectors for each climate division after fitting the climatic division composites with a 24-month harmonic. In this approach, vectors point towards periods of wetter-than-normal temperature, corresponding to the positive phase of the cycle. The actual direction of the ENSO-temperature relationship is determined by examining these composites. This study focuses on regions in the study area that exhibit significant and sustained ENSO-temperature correlations over many months. Isolated or transient relationships in individual climatic divisions are not considered further. Mapping the harmonic vectors provides a method to identify geographical areas with coherent responses to ENSO. Regions with the strongest coherence were selected based on the ratio of the average vector magnitude to the arithmetic mean of all vector magnitudes.

$$\text{Spatial Coherence} = \frac{\text{sqrt}((\sum V\cos\theta)^2 + (\sum V\sin\theta)^2)}{\sum V} \tag{4}$$

The denominator contains the arithmetic average value of the vector magnitudes, and the numerator is the average vector magnitude of all harmonic vectors in the chosen regions. V and θ are magnitude and angle of the vector. This analysis is restricted to areas where coherence values reach or exceed 0.80 (Ropelewski and Halpert, 1986), excluding regions with high-amplitude but inconsistent phase relationships across climate division. Index Time Series (ITS) are obtained by spatiotemporally averaging temperature values during signal seasons across record years and candidate regions. ITS values represent the temporal consistency rates of ENSO-related temperature signals. The temporal consistency rates are determined by the proportion of years showing ENSO signals in ITS compared to total ENSO event years, identifying core regions with reliable ENSO-temperature relationships. The study also investigates extreme temperature events associated with ENSO, following methods outlined by Ropelewski et al. (1986) to explore the climatic connection between ENSO events and extreme temperature anomalies. Years with ENSO-related extreme temperatures are identified within signal seasons. Index Time Series (ITS) data are ranked, normalized across the dataset, and converted into probability time series to categorize extreme event levels. The lowest and highest ITS values are assigned probabilities of 20% and 80%, respectively (Kahya and Dracup, 1994).

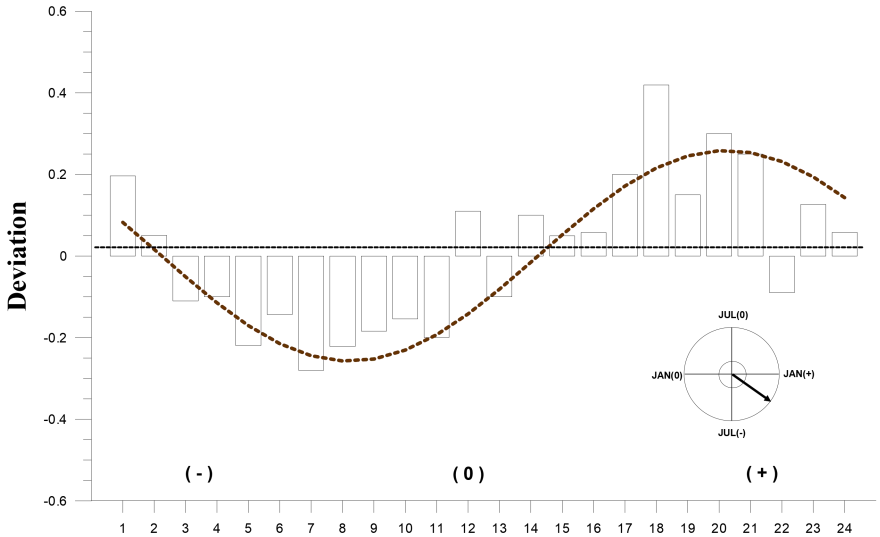

Figure 3. A first harmonic fit to the temperature ENSO composite for the climate division CD-11. The amplitude and the phase of the first harmonic are presented as a harmonic dial (the lower right).

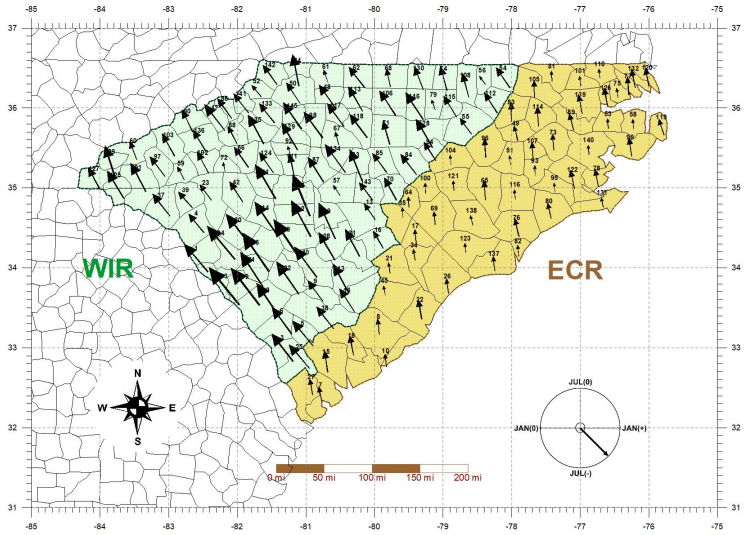

(a)

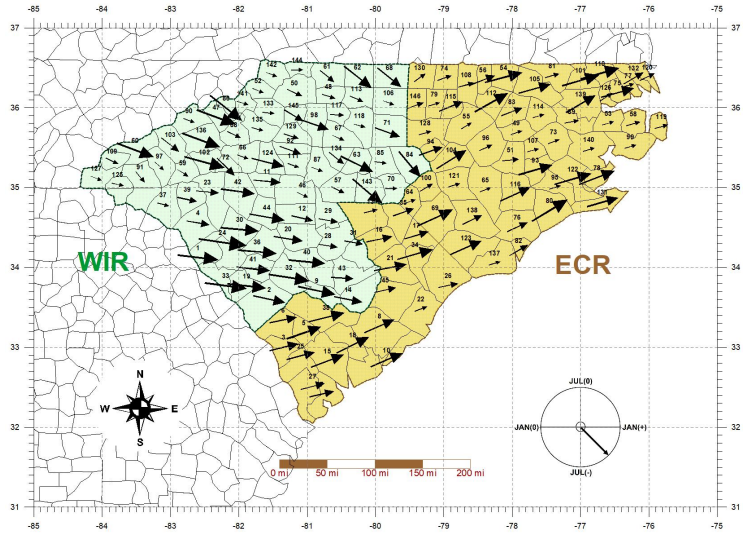

(b)

Figure 4. Harmonic dial map based on the first harmonic of the 2-year El Niño (**a**) and La Niña (**b**) composites. Scale for the direction of arrows: south, July (−); west, January (0); north, July (0); and east, January (+). The magnitude of arrows is proportional to the amplitude of the harmonics.

Composite analysis aggregates temperature data from ENSO years (both El Niño and La Niña events) to identify general patterns. By averaging temperatures over multiple years with similar ENSO conditions, composite analysis highlights typical temperature responses during warm and cold ENSO phases. This method captures broad trends and distinguishes between warm and cold ENSO influences on local temperatures. However, composite analysis can oversimplify temperature variability by averaging out unique yearly anomalies, potentially obscuring less common but important variations. Additionally, it assumes that each ENSO event affects the region similarly, although other climatic factors might cause different responses in individual years. On the other hand, Harmonic analysis decomposes the temperature data into sinusoidal cycles, allowing for the identification of periodic temperature patterns tied to ENSO cycles. The method is particularly useful for capturing seasonal and cyclic variations that align with the ENSO phases. This approach helps pinpoint regions with strong, consistent responses to ENSO events and aids in identifying the timing of temperature anomalies within the annual ENSO cycle. However, harmonic analysis relies on periodic consistency, which may not capture irregularities or abrupt changes in ENSO patterns. Furthermore, it may fail to account for non-ENSO-related temperature anomalies that do not fit into the sinusoidal pattern, potentially misrepresenting the effect of ENSO in areas with complex temperature variability. In summary, while composite and harmonic analyses offer valuable insights into ENSO-induced temperature patterns, they each have limitations. These include assumptions of linearity and challenges in isolating ENSO effects

from other climate drivers. Recognizing these limitations is crucial for interpreting the findings accurately and understanding the scope of ENSO's influence on local temperatures in the Southeastern US.

2.4. Comparative Analyses

ENSO-related temperature responses are evaluated using the hypergeometric distribution test. Haan (1977) developed this test to determine the probability of obtaining at least m successes in n trials from a population of size N, where there are k successes. This cumulative probability provides a measure of the relationship's statistical significance for both extreme phases of ENSO. Kahya et al. (1994) adapted the hypergeometric test to assess average values and extreme high/low events. In this study, two scenarios (A and B) are considered based on how success is defined. Scenario A defines success as years where the ITS value in relation to ENSO forcings is higher or lower than the median. Scenario B defines success as years where the ITS values fall within the higher or lower 20% of the distribution. Annual cycle analysis is employed to compare the effects of warm and cold phases of ENSO on temperature anomalies, focusing on both the trend and magnitude of the signal over the year. Monthly temperature time series are converted to modular coefficients for the annual cycle analysis, which standardizes data by removing dispersed variance and mean values. These coefficients express the time series data as percentages relative to the annual average, helping to assess whether extreme ENSO phases enhance or diminish temperature. Seasonal cross-correlation coefficients are computed to analyze ENSO-related temperature signals, examining both positive and negative correlations. Five categorized SOI datasets, representing ENSO indices, are correlated with percentile ranked probability of monthly temperature time series. The resulting correlation coefficient values represent the strength and direction of the climatic links between ENSO forcing and seasonal temperature patterns. Further details on data processing and correlation procedures are provided in the initial section of this study.

3. Results and Discussion

3.1. Temperature Response to El Niño

Figure 4(a) displays a harmonic dial map presenting candidate regions identified through composite and harmonic analyses. A vector map for temperature indicates two coherent ENSO-responsive regions in the study area: Western Inland Region (WIR) and Eastern Coastal Region (ECR). Table 2 presents composite temperature indices for each region, affirming their ENSO-related response. Detailed analysis of these indices reveals distinct wet season patterns within the ENSO cycle across these regions. Figure 5(a) illustrates the time series of November (0) to April (+) temperature indices averaged across all stations in the WIR region, highlighting consistent below-average temperature during 21 out of 29 ENSO events. Notably, 11 instances with index values meeting or exceeding the lowest ITS limit (20%) corresponded to ENSO, contrasting with only one occurrence at the highest ITS limit (80%). Temporal consistency and spatial coherence were measured at 0.72 and 0.98, respectively. Figure 6(a) depicts the time series of January (+) to May (+) temperature indices for the ECR region, indicating below-average temperature during 22 out of 29 ENSO events. While 11 ENSO years saw index values surpassing the 20% threshold, negative values of similar magnitude also occurred during 14 non-ENSO years. Only two ENSO-related seasons fell within the highest ITS limit (80%). Temporal consistency and spatial coherence were 0.76 and 0.97.

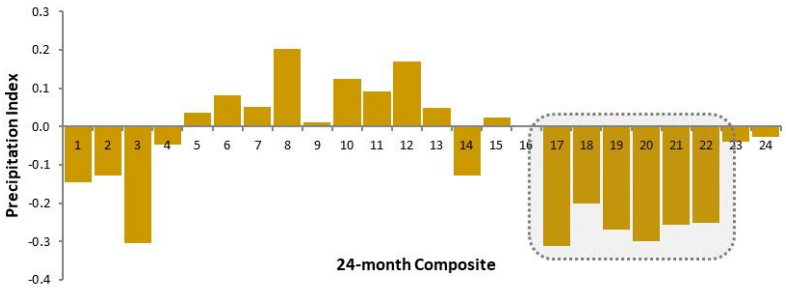

(a)

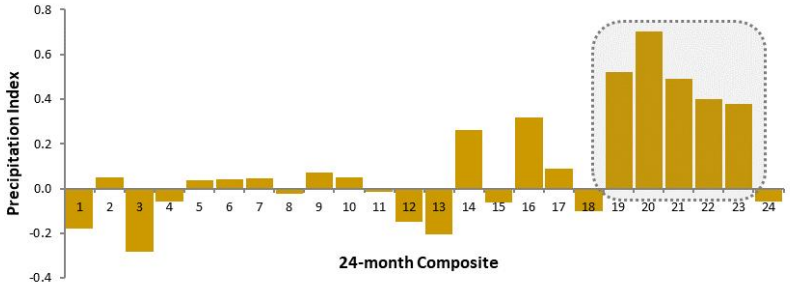

(b)

Figure 5. El Niño (**a**) and La Niña (**b**) aggregate composite for the candidate WIR region. The dashed line box delineates the season of possible ENSO-related responses.

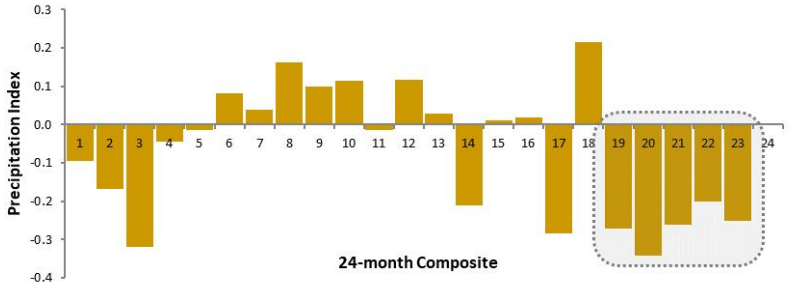

(a)

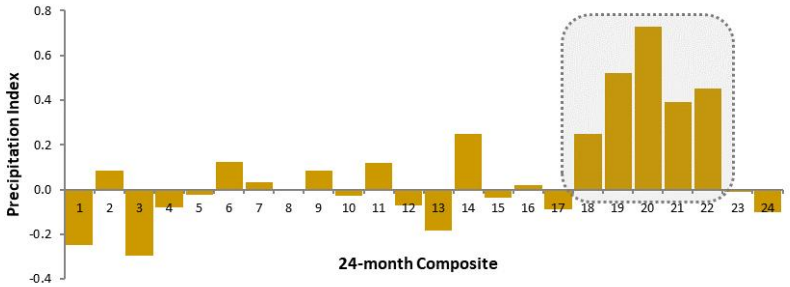

(b)

Figure 6. El Niño (a) and La Niña (b) aggregate composite for the candidate ECR region. The dashed line box delineates the season of possible ENSO-related responses.

Table 2. Properties of the Candidate Regions (El Niño events)

Core Region	Signal Season	Coherence Rate	Total Episode	Occurrence Episode	Consistency Rate	Extreme Events
WIR	Nov (0) – Apr (+)	98%	29	21	72 %	11
ECR	Jan (+) – May (+)	97%	29	22	76 %	11

3.2. Temperature Response to La Niña

For the 22 La Niña events, representing the cold ENSO phase, monthly temperature data underwent composite and harmonic analyses. Figure 4(b) displays a map of harmonic dial vectors illustrating consistent temperature responses in the Western Inland Region (WIR) and Eastern Coastal Region (ECR). ENSO composite temperature indices for each region are detailed in Figure 5 (b) and 6(b), with Table 3 summarizing the results of these analyses. In the WIR region, standardized temperature departures averaged across all climate divisions from January (+) to May (+) indicate positive departures for 18 out of 22 La Niña events (Figure 5b). Index values meeting or falling above the highest ITS limit (80%) occurred in 6 La Niña years, whereas occurrences at the lowest ITS limit (20%) were associated

with only two La Niña years. Spatial coherence and temporal consistency were measured at 0.97 and 0.82. Within the ECR region, the period from December (0) to April (+) shows positive temperature departures for 19 out of 22 La Niña events (Figure 6b). Index values above or equal to the highest ITS limit (80%) were observed in 7 La Niña years, with none of these years reaching the extreme conditions defined by the lowest ITS limit (20%). Temporal consistency and spatial coherence were 0.86 and 0.99.

Table 3. Properties of the Candidate Regions (La Niña events).

Core Region	Signal Season	Coherence Rate	Total Episode	Occurrence Episode	Consistency Rate	Extreme Events
WIR	Jan (+) – May (+)	97%	22	18	82 %	6
ECR	Dec (0) – Apr (+)	99%	22	19	86 %	7

3.3. Comparative Analysis of El Niño and La Niña

The hypergeometric distribution was used to assess the likelihood of random hot or cold seasons occurring during ENSO event years. In Case A, both events showed very low probabilities (less than 0.002). In Case B, probabilities were similarly low for both extreme event phases. The occurrence of extreme temperature conditions predominantly aligns with ENSO events over the 125-year period. The results in Table 4 and 5 consistently reflect high confirmation rates for temporal consistency of signals (72-76% for El Niño events and 82-86% for La Niña events), indicating that relationships depicted in composite analyses are attributable to nonrandom mechanisms such as tropical thermal anomalies. Monthly temperature time series were converted to modular coefficients for conducting annual cycle analysis. ENSO composites were derived from these series and plotted alongside the regional annual cycle as shown in Figures 9 and 10. These figures reveal two primary patterns: during El Niño events, enhanced temperature during the ENSO year is followed by decreased temperature into the subsequent year; during La Niña events, suppressed amplitude during the ENSO year precedes increased amplitude into the following year. These amplitude variations coincide with previously identified high and low signal seasons in the two core regions. Additionally, distinct opposite trends in monthly temperature patterns between the warm and cold ENSO composites were observed over a 2-year period. Overall, the findings show that tropical thermal anomalies modulate monthly temperature patterns in the study area, influencing either increases or decreases. Table 6 presents cross-correlation coefficient results, indicating the intensity and direction of correlation between ENSO forcing and suppressed patterns. The cross-correlation analysis involved large-scale climate indicators and seasonal suppressed time series, utilizing five categorized Southern Oscillation Index (SOI) datasets and percentile-ranked probabilities. Significant correlations (at the 0.05 significance level) were found between seasonal suppressed anomalies and both extreme phases of SOI. For strong warm phase SOI conditions, the highest positive (negative) correlation coefficients were observed at lag-0 (lag-3 and lag-4) across the two core regions. Conversely, for strong cold phase SOI conditions, the highest negative (positive) correlation coefficients were found at lag-0 (lag-3) across the two core regions. These results indicate that stronger warm (cold) phases of ENSO correspond to increased (decreased) suppressed occurring with lag times of 0, 3, and 4 (0 and 3) seasons in the study area.

Table 4. Probabilistic assessments for significance level based on the hypergeometric distribution (El Niño events).

Case	Region	N	k	n	m	Probability
A	WIR	125	60	29	21	0.002
	ECR	125	61	29	22	0.003
B	WIR	125	25	25	13	0.002
	ECR	125	25	25	11	0.002

Table 5. Probabilistic assessments for significance level based on the hypergeometric distribution (La Niña events).

Case	Region	N	k	n	m	Probability
A	WIR	125	63	22	18	0.001
	ECR	125	64	22	19	0.000
B	WIR	125	25	22	6	0.041
	ECR	125	25	22	7	0.037

Table 6. Cross-correlation coefficients with respect to regions

Core Region		Strong El Niño SOI					Normal Condition					Strong La Niña SOI				
		lag-0	lag-1	lag-2	lag-3	lag-4	lag-0	lag-1	lag-2	lag-3	lag-4	lag-0	lag-1	lag-2	lag-3	lag-4
El Niño	WIR	**0.49**	-0.09	0.14	**-0.83**	**-0.52**	0.00	-0.07	0.03	0.00	0.08	**-0.51**	0.03	-0.20	**0.84**	-0.01
	ECR	**0.48**	-0.31	-0.01	**-0.74**	**-0.56**	-0.02	-0.07	0.02	0.01	0.09	**-0.53**	0.05	-0.21	**0.87**	0.04
La Niña	WIR	**0.50**	-0.12	0.14	**-0.83**	**-0.52**	0.00	-0.07	0.03	0.00	0.09	**-0.50**	0.04	-0.19	**0.84**	-0.03
	ECR	**0.47**	-0.20	0.04	**-0.77**	**-0.54**	-0.02	-0.07	0.02	0.00	0.09	**-0.53**	0.02	-0.22	**0.85**	0.05

3.4. Discussion

The study provides a detailed comparison of El Niño and La Niña effects on local temperature patterns in the Southeastern US, highlighting distinct but complementary influences from both ENSO phases. During El Niño years, temperatures in the Western Inland Region (WIR) and Eastern Coastal Region (ECR) show below-normal temperatures across the cool season (from November to May). These negative temperature anomalies are stronger and more coherent than those during non-ENSO years. Spatial coherence rates are high and the WIR region experiences the most significant temperature drops. The temporal consistency is slightly lower than during La Niña. In contrast, La Niña leads to above-normal temperatures in both regions, particularly from December to May. The temperature increases during La Niña years tends to be less pronounced than the cooling seen during El Niño years, though spatial coherence is still high. The temporal consistency of temperature anomalies is slightly higher in La Niña years. The comparative analysis reveals that El Niño tends to induce more consistent and stronger negative temperature anomalies, while La Niña's positive temperature responses are slightly weaker but more temporally stable. Both phases, however, significantly impact local temperature patterns, with El Niño exerting a greater cooling effect and La Niña causing moderate warming. Temperature patterns in both phases display high spatial coherence across the Southeastern US, but with opposite temperature trends (cooling during El Niño and warming during La Niña). Thus, while both phenomena disrupt normal temperature patterns, El Niño's cooling effects are more intense, whereas La Niña's warming is more consistent but less extreme.

Figures 4 (a)–8(a) illustrate that this study identifies decreased temperature during El Niño events in the WIR and ECR regions in early fall (0) and spring (+) seasons. Particularly in the WIR region, the magnitude of this negative deviation from normal temperature during El Niño years significantly surpasses non-El Niño years. Conversely, Figures 4(b)–8(b) reveal a contrasting pattern during La Niña, where monthly temperature anomalies indicate above normal conditions across the WIR and ECR regions from fall (0) through spring (+) seasons. Notably, the positive anomaly during La Niña years in the WIR region is markedly higher compared to non-event years. Rasmusson et al. (1983) revealed a strengthened subtropical jet stream displaced southward from its normal position in the extreme phases of ENSO forcing. This intensification of the jet stream brought winter storms causing cooling events in the southern United States. The temperature response in the southern US to the ENSO forcing is consistent with the findings by Ropelewski et al. (1986), Douglas et al. (1981). Ropelewski et al. (1986) documented that the temperature response to ENSO forcing may be more easily explained in terms of direct or shorter-range effects associated with the developed subtropical jet stream and warmer than normal surface water over the tropical Pacific Ocean. In addition, they explained that the region has shown abnormal cold temperatures related to previous ENSO episodes. Douglas et al. (1981) suggested that the ENSO-related temperature signal may be an indication of a more apparent linkage to ENSO events than a PNA teleconnection pattern (Pacific North American). Active ENSO-related convection is common in the tropical Pacific Ocean and southern United States. This convection has been connected to strong westerlies in the southern US including Gulf of Mexico as shown in the previous study by Arkin (1982) and, hence, a tendency for more frequent cooling events in the southern regions of United States.

This possible apparent linkage to the ENSO-related forcing may account for the consistent temperature response over the southeastern United States. In ENSO years, the occurrence of warm and cold SST (sea surface temperatures) over the central and eastern tropical Pacific Ocean induces large-scale atmospheric circulations in the middle latitude resulting from complex atmosphere-ocean coupled interactions. Consequently, these ENSO-related coupled circulations perturb abnormal temperature fluctuations over the Southeastern United States.

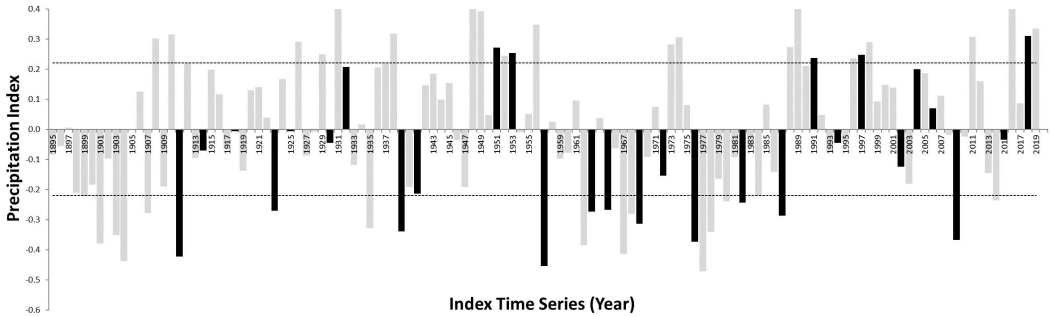

(a)

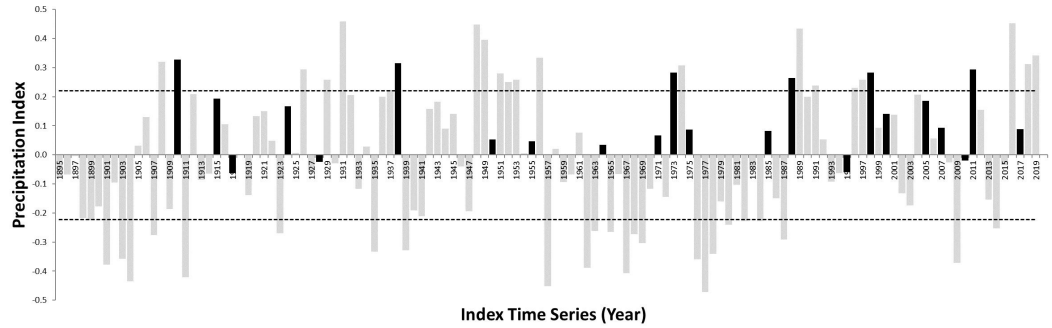

(b)

Figure 7. The index time series for the WIR region for the season previously detected. El Niño (**a**) and La Niña (**b**) years are shown by solid bars. The dashed horizontal lines are the upper (80%) and lower (20%) limits for ITS.

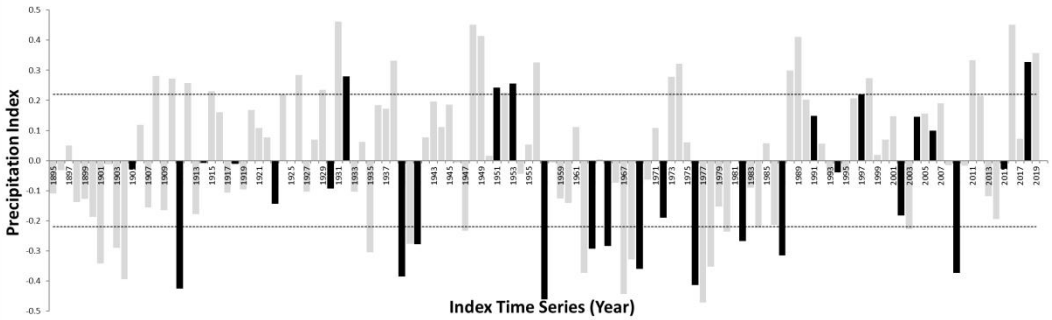

(a)

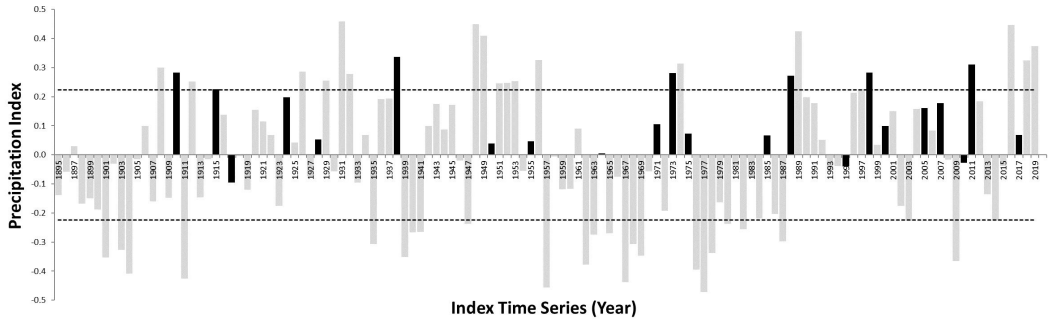

(b)

Figure 8. The index time series for the ECR region for the season previously detected. El Niño (**a**) and La Niña (**b**) years are shown by solid bars. The dashed horizontal lines are the upper (80%) and lower (20%) limits for ITS.

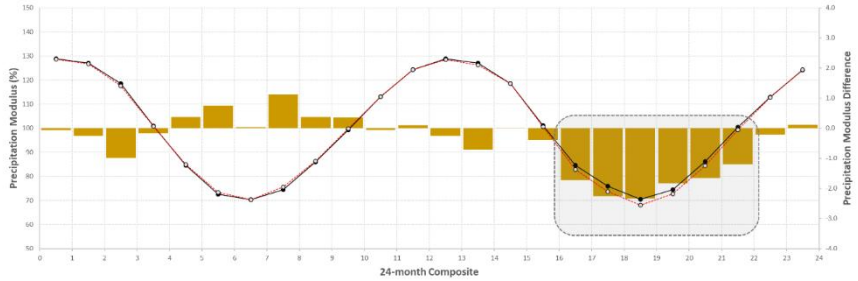

(a)

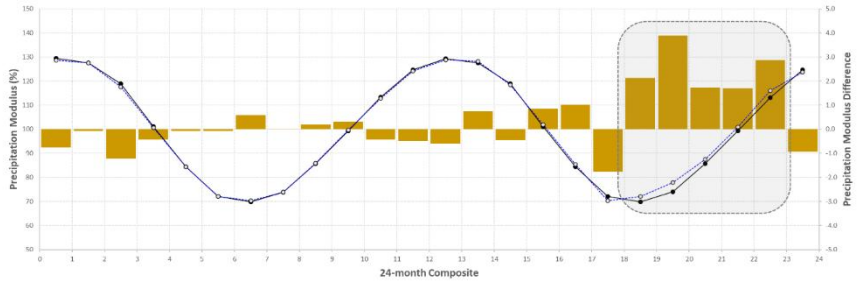

(b)

Figure 9. The comparison between El Niño (**a**) and La Niña (**b**) composite cycles (shown by dashed line) and annual cycles (shown by solid line) of the WIR regions, based on modular coefficients. Dashed boxes indicate the beginning and end months of the SO signal season.

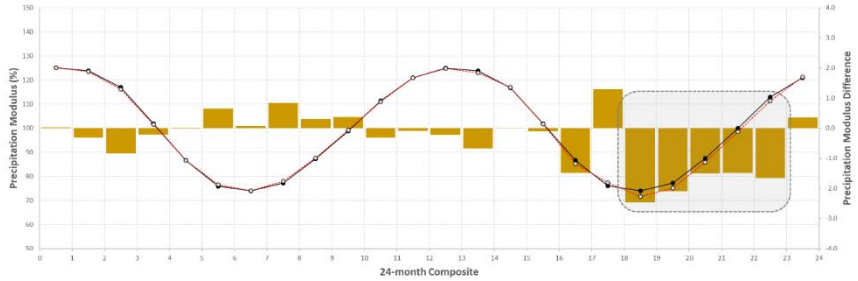

(a)

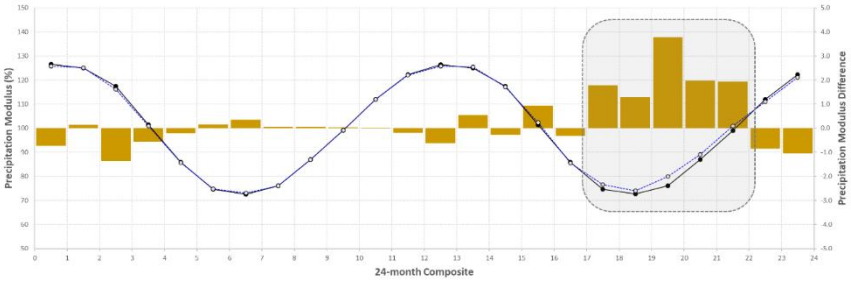

(b)

Figure 10. The comparison between El Niño (**a**) and La Niña (**b**) composite cycles (shown by dashed line) and annual cycles (shown by solid line) of the ECR regions, based on modular coefficients. Dashed boxes indicate the beginning and end months of the SO signal season.

4. Summary and Conclusions

This study examined the teleconnection between ENSO thermal impacts on monthly temperature anomalies in the study area using a series of empirical and statistical analyses including composite-harmonic analysis, cross-correlation analysis, and annual cycle analysis, The resultant findings, detailed in Tables 2 to 3, categorized the study area into two core regions: Western Inland Region (WIR) and Eastern Coastal Region (ECR). They demonstrated strong spatial coherence and temporal consistency, highlighting significant spatial extent and intensity of temperature responses to ENSO phenomena. The key findings are as follows. Firstly, during El Niño events, temperature patterns are consistently below normal in the WIR and ECR regions across the signal seasons from November (0) to April and January (+) to May (+). Spatial coherence ranges from 0.97 to 0.98, and temporal consistency rates are between 0.72 and 0.86. The WIR region exhibits the highest negative temperature departure magnitude during El Niño years. Conversely, during La Niña events, temperature patterns show above normal in the WIR and ECR regions during the periods from January (+) to May (+) and December (0) to April (+), respectively. Spatial coherence rates range from 0.97 to 0.99, and temporal consistency rates ranges from 0.82 to 0.86. Additionally, comparative analyses between warm and cold phases of ENSO events highlight a strong correlation between ENSO and temperature responses, with opposing trends in monthly temperature anomalies (negative during warm phase and positive during cold phase). El Niño events show more significant below-normal temperature anomalies compared to above-normal patterns during La Niña events. Annual cycle analysis reveals that the annual temperature cycle in the study area is influenced by tropical heating and cooling anomalies in sea surface temperatures, resulting in fluctuations that either increase or decrease temperature. Cross-correlation coefficient analyses indicate the highest correlation values in lag-0, 3, and 4 (lag-0 and 3) cases across the two core regions for strong warm (cold) phase SOI conditions. This suggests that stronger warm (cold) phase of ENSO forcing lead to be decreased (increased) temperature with lag times of 0, 3, and 4 (0 and 3) seasons across the study area. In conclusion, this study identifies distinct local temperature responses to El Niño and La Niña phenomena across the Southeastern US. Incorporating multiple climate variables can complicate the analysis, especially if the goal is to derive specific insights into ENSO's direct influence on local temperature patterns. Focusing on temperature simplifies the model or study design, enabling a more precise quantification of ENSO's thermal effects. By focusing on temperature alone, this study captures the local thermal impact of ENSO more directly and allows for clearer insights into how each phase of ENSO might influence temperature variability in the Southeastern US. This can serve as a foundation for additional studies that may later integrate other variables, such as precipitation, once the direct ENSO-temperature relationship is well-established.

References

Arkin, P. A., 1982. The relationship between interannual variability in the 200 mb tropical wind field and the Southern Oscillation. Mon. Wea. Rev.,110, 1393–1404. https://doi.org/10.1175/1520-0493(1982)110<1393:TRBIVI>2.0.CO;2

Berlage, H.P., 1966. The Southern Oscillation and world weather. Meteor. Inst. Meded. Verh., 88, 152pp.

Bradley, R.S., Diaz, H.F., Kiladis, G.N., Eischeid, J. K., 1987. ENSO signal in continental temperature and precipitation records, Nature, 327, 497-501. doi.org/10.1038/327497a0

Davey, M.K., Brookshaw A., Inesona, S., 2014. The probability of the impact of ENSO on precipitation and near-surface temperature. Climate Risk Management, Vol. 1, 5-24. doi.org/10.1016/j.crm.2013.12.002

Douglas, A.E., Englehart, P.J., 1981. On a statistical relationship between autumn rainfall in the central equatorial pacific and subsequent winter precipitation in Florida. Mon. Weather Rev., 109, 2377-2382.

doi.org/10.1175/1520-0493(1981)109<2377:OASRBA>2.0.CO;2.
Haan, C.T., 1977. Statistical Methods in Hydrology. Iowa State University Press, Ames, IA.
Halpert MS, Ropelewski CF. 1992. Surface temperature patterns associated with the Southern Oscillation. *Journal of Climate* 5: 557–593. doi.org/10.1175/1520-0442(1992)005<0577:STPAWT>2.0.CO;2
Kahya, E., Dracup, J.A., 1994. The influences of Type 1 El Niño and La Niña events on streamflows in the Pacific southwest of the United States. Journal of Climate, 7: 965–976. doi.org/10.1175/1520-0442(1994)007<0965:TIOTEN>2.0.CO;2.
Kemarau R.A., Eboy, O.V., 2022. The Impact of El Niño–Southern Oscillation (ENSO) on Temperature: A Case Study in Kuching, Sarawak, Malaysian Journal of Social Sciences and Humanities, Vol. 6, Issue 1, 289-297. doi.org/10.47405/mjssh.v6i1.602
Kiladis, G.N., Diaz, H.F., 1989. Global climatic anomalies associated with extremes in the Southern Oscillation. Journal of Climate, 2, 1069–1090. doi.org/10.1175/1520-0442(1989)002<1069:GCAAWE>2.0.CO;2.
Kiladis, G.N., van Loon, H., 1988. The Southern Oscillation. Part VII: Meteorological Anomalies over the Indian and Pacific Sectors Associated with the Extremes of the Oscillation. Monthly Weather Review, Vol. 116, Issue 1, 120-136. doi.org/10.1175/1520-0493(1988)116<0120:TSOPVM>2.0.CO;2
Lee, J. H., Julien, P. Y., 2016. ENSO impacts on temperature over South Korea. International Journal of Climatology, 36, 3651-3663. doi.org/10.1002/joc.4581
Rasmusson, E.M., Carpenter, T.H., 1983. The relationship between eastern equatorial Pacific sea surface temperatures and rainfall over India and Sri Lanka. Mon. Wea. Rev., 111, 517–528. doi.org/10.1175/1520-0493(1983)111<0517:TRBEEP>2.0.CO;2.
Rasmusson, E.M., Wallace, J.M., 1983. Meteorological aspects of the El Niño/southern oscillation. Science, 222, 1195–1202. doi.org/10.1126/science.222.4629.1195.
Redmond, K.T., Koch, R.W., 1991. Surface climate and streamflow variability in the western United States and their relationship to large-scale circulation indices. Water Resources Research, Vol. 27, Issue 9, 2381-2399. doi.org/10.1029/91WR00690.
Ropelewski, C.F., Halpert, M.S., 1986. North American precipitation and temperature patterns associated with El-Niño-Southern oscillation (ENSO). Mon. Weather Review, 114, 2165–2352. doi.org/10.1175/1520-0493(1986)114<2352:NAPATP>2.0.CO;2.
Ropelewski, C.F., Halpert, M.S., 1987. Global and regional scale precipitation patterns associated with the El Niño/Southern Oscillation. Mon. Wea. Rev., 115, 1606–1626. doi.org/10.1175/1520-0493(1987) 115<1606:GARSPP>2.0.CO;2.
Ropelewski, C.F., Halpert, M.S., 1989. Precipitation patterns associated with the high index phase of the southern oscillation. Journal of Climate, 2, 268–284. doi.org/10.1175/1520-0442(1989)002<0268:PPAWTH>2.0. CO;2.
Tamaddun, K.A., Kalra, A., Bernardez, M., Ahmad, S., 2019. Effects of ENSO on Temperature, Precipitation, and Potential Evapotranspiration of North India's Monsoon: An Analysis of Trend and Entropy. Water, Vol. 11, Issue 2, 189. doi.org/10.3390/w11020189
van Loon, H., Madden, R.A., 1981. The Southern Oscillation. Part I: Global Associations with Pressure and Temperature in Northern Winter. Monthly Weather Review, Vol. 109, Issue 6, 1150-1162. doi.org/10.1175/1520-0493(1981)109<1150:TSOPIG>2.0.CO;2
Viet, L.V., 2021. Development of a new ENSO index to assess the effects of ENSO on temperature over southern Vietnam. Theoretical and Applied Climatology, Vol. 144, 1119-1129. 10.1007/s00704-021-03591-3
Walker, G.T., 1923. Correlation in seasonal variations of weather, V III, A preliminary study of world weather, Mem. Indian Meteorol. Dep., 24, 75-131.
Walker, G.T., Bliss, E.W., 1932. World Weather V. Mem. Roy. Meteor. Soc., 4 (36), 53–84.
Wilks, D. S., 1995. Statistical Methods in Atmospheric Sciences. Academic Press, 330-334.
WMO, 2014. El Niño/Southern Oscillation. WMO-No. 1145, 2–4.